AFRL-RY-HS-TR-2009-0017

SEMICONDUCTOR TERAHERTZ TECHNOLOGY

Gregory Sun

University of Massachusetts/Boston
100 Morrissey Boulevard, Room 80
Boston, MA 02125-3300

15 June 2009

Final Report

AIR FORCE RESEARCH LABORATORY
Sensors Directorate
Electromagnetics Technology Division
80 Scott Drive
Hanscom AFB MA 01731-2909

NOTICE AND SIGNATURE PAGE

Using Government drawings, specifications, or other data included in this document for any purpose other than Government procurement does not in any way obligate the U.S. Government. The fact that the Government formulated or supplied the drawings, specifications, or other data does not license the holder or any other person or corporation; or convey any rights or permission to manufacture, use, or sell any patented invention that may relate to them.

This report was cleared for public release by the Electronic Systems Center Public Affairs Office for the Air Force Research Laboratory Electromagnetic Technology Division and is available to the general public, including foreign nationals. Copies may be obtained from the Defense Technical Information Center (DTIC) (http://www.dtic.mil).

AFRL-RY-HS-TR-2009-0017 HAS BEEN REVIEWED AND IS APPROVED FOR PUBLICATION IN ACCORDANCE WITH ASSIGNED DISTRIBUTION STATEMENT.

Richard Soref

RICHARD SOREF
Contract Monitor

David F. Bliss

DAVID F. BLISS
Acting Chief, Optoelectronic Technology Branch

M. N. Alexander

MICHAEL N. ALEXANDER
Technical Advisor
Electromagnetic Technology Division

This report is published in the interest of scientific and technical information exchange, and its publication does not constitute the Government's approval or disapproval of its ideas or findings.

REPORT DOCUMENTATION PAGE

Form Approved OMB No. 0704-0188

1. REPORT DATE *(DD-MM-YY)*	2. REPORT TYPE	3. DATES COVERED *(From - To)*
15-June-2009	Final Report	12 Apr 07 – 15 Apr 09

4. TITLE AND SUBTITLE

Semiconductor Terahertz Technology

5a. CONTRACT NUMBER
FA8718-07-C-0030

5b. GRANT NUMBER

5c. PROGRAM ELEMENT NUMBER
61102F

6. AUTHOR(S)

Gregory Sun

5d. PROJECT NUMBER
2305

5e. TASK NUMBER
HC

5f. WORK UNIT NUMBER
0C

7. PERFORMING ORGANIZATION NAME(S) AND ADDRESS(ES)

University of Massachusetts/Boston
100 Morrissey Boulevard, Room 80
Boston, MA 02125-3300

8. PERFORMING ORGANIZATION REPORT

9. SPONSORING / MONITORING AGENCY NAME(S) AND ADDRESS(ES)

Electromagnetics Technology Division Source Code: 437890
Sensors Directorate
Air Force Research Laboratory
80 Scott Drive
Hanscom AFB MA 01731-2909

10. SPONSOR/MONITOR'S ACRONYM(S)

11. SPONSOR/MONITOR'S REPORT NUMBER(S)
AFRL-RY-HS-TR-2009-0017

12. DISTRIBUTION / AVAILABILITY STATEMENT

Approved for Public Release; Distribution Unlimited. 1 February 2007. Other requests for this document shall be referred to AFRL/RYHC, 80 Scott Drive, Hanscom AFB, MA 01731-2909. Cleared for Public Release by 66ABW/PA, Case Number: 66ABW-2009-0922, 10 August 2009.

13. SUPPLEMENTARY NOTES

The U. S. Government is joint author of this work and has the right to use, modify, reproduce, release, perform, display, or disclose the work.

14. ABSTRACT

During this contract, we have investigated the THz laser source based on group-IV elements and their alloys that can be developed on Si substrates. The design work focused on the structure of the so-called quantum cascade laser (QCL). Specifically, we designed a $Ge/Ge_{0.76}Si_{0.19}Sn_{0.05}$ QCL using intersubband transitions at L-valleys of the conduction band which has a "clean" offset of 150meV situated below other energy valleys (Γ, X). The entire structure is strain free because the lattice-matched Ge and $Ge_{0.76}Si_{0.19}Sn_{0.05}$ layers are to be grown on a relaxed Ge buffer layer on a Si substrate. Longer lifetimes due to the weaker scattering of nonpolar optical phonons reduce threshold current and potentially lead to room temperature operation. For the work on phonon waveguides, we have studied the characteristics of waveguides using interface phonon polaritons to confine far-infrared radiation within a sub-wavelength semiconductor layer. We have identified spectral operating regions within the Restrahlen band of a cladding layer that offers advantages over both traditional dielectric and metal clad waveguides. We showed that proposed waveguides can be used for far-infrared low-threshold QCLs. The report is devided into two parts, one for the design of group-IV QCLs and the other for the phononic waveguides.

15. SUBJECT TERMS

Quantum cascade laser, germanium, germanium-tin, terahertz

16. SECURITY CLASSIFICATION OF:			17.LIMITATION OF ABSTRACT	18.NUMBER OF PAGES	19a. NAME OF RESPONSIBLE PERSON
a. REPORT	b. ABSTRACT	c.THIS PAGE			Richard Soref
Unclassified	Unclassified	Unclassified	SAR	22	19b. TELEPHONE NUMBER *(include area code)* (781) 377-2380

Standard Form 298 (Rev. 8-98)
Prescribed by ANSI Std. Z39.18

Table of Contents

List of Figures

Summary

During this contract, we have investigated the THz laser source based on group-IV elements and their alloys that can be developed on Si substrates. The design work focused on the structure of the so-called quantum cascade laser (QCL). Specifically, we designed a $Ge/Ge_{0.76}Si_{0.19}Sn_{0.05}$ QCL using intersubband transitions at *L*-valleys of the conduction band which has a "clean" offset of 150meV situated below other energy valleys (Γ, X). The entire structure is strain free because the lattice-matched Ge and $Ge_{0.76}Si_{0.19}Sn_{0.05}$ layers are to be grown on a relaxed Ge buffer layer on a Si substrate. Longer lifetimes due to the weaker scattering of nonpolar optical phonons reduce threshold current and potentially lead to room temperature operation. For the work on phonon waveguides, we have studied the characteristics of waveguides using interface phonon polaritons to confine far-infrared radiation within a sub-wavelength semiconductor layer. We have identified spectral operating regions within the Restrahlen band of a cladding layer that offers advantages over both traditional dielectric and metal clad waveguides. We showed that proposed waveguides can be used for far-infrared low-threshold QCLs. The report is devided into two parts, one for the design of group-IV QCLs and the other for the phononic waveguides.

I. Group-IV QCLs

Electrically pumped Si-based lasers have long been sought because they serve as light sources for monolithic integration of Si electronics with photonic components on the same Si wafer. Unfortunately, Si has not been a material of choice for luminescence applications owing to its indirect bandgap. It has been proposed that lasers based on intersubband transitions (IST) in SiGe quantum wells (QWs) could circumvent the issue of bandgap indirectness.[1] In addition, SiGe QWs being nonpolar material are expected to have longer intersubband lifetimes that reduce threshold current and to be free from the reststrahl absorption that is found in III-V quantum cascade lasers (QCLs).

I.1 Brief overview of Si-based QCL development

Various groups have obtained electroluminescence from Si-rich Si/SiGe quantum cascade structures,[2-4] but lasing has eluded researchers up to now. Those efforts all have one scheme in common: holes instead of electrons are used for IST because most of the band offset between the Si-rich SiGe QWs and the Si barriers is in the valence band. There are a number of difficulties associated with valence band Si/SiGe QCLs. First, the strong mixing of heavy-hole, light-hole, and split-off bands makes the QCL design exceedingly cumbersome and adds a great degree of uncertainty. Second, the large effective mass of heavy holes hinders carrier injection efficiency and leads to small ISB oscillator strength between laser states. Third, for any significant band offset needed to implement QCLs, lattice-mismatch-induced strain in SiGe QWs is likely to limit total structural thickness in order to avoid generating structural defects. Recently, a new conduction intersubband approach was proposed to construct a Ge/SiGe QCL using strained Ge QWs and SiGe alloy barriers.[5] That structure effectively avoids the valence band complexity, but the two Δ_2-valleys along the (001) growth direction are still entangled

with the *L*-valleys in the conduction band, leading to design complexity and potentially creating additional nonradiative decay channels for the upper laser state.

I.2 Choice of $Ge/Ge_{1-x-y}Si_xSn_y$ materials for QCLs

To circumvent the problems of strain developed in the Si/SiGe heterostructures and entanglement of energy valleys in the conduction band, we took the approach of employing $Ge/Ge_{1-x-y}Si_xSn_y$ heterostructures to develop *L*-valley QCLs. $Ge_{1-x-y}Si_xSn_y$ alloys have been studied for the possibility of forming direct bandgap semiconductors.[6-9] Since the first successful growth of this alloy,[10] device- quality epilayers with a wide range of alloy contents have been achieved. Incorporation of Sn provides the opportunity to engineer separately the strain and band structure since we can vary the Si (x) and Sn (y) compositions independently. Certain alloy compositions of this material system offer three advantages: (1) the possibility of a "cleaner" conduction band lineup in which the *L*-valleys in both well and barrier sit below other valleys (Γ, X), (2), an electron effective mass along the (001) growth direction that is much lower than the prior heavy-hole mass, and (3) a lattice-matched structure that is entirely strain free. In addition, recent advances in the direct growth of Ge layer on Si provide a relaxed matching buffer layer on a Si substrate upon which the strain-free QCL is grown.[11]

I.3 $Ge/Ge_{1-x-y}Si_xSn_y$ conduction band structure

Since band offsets between ternary Sn-containing alloys and Si or Ge are not known experimentally, we have calculated the conduction band minima for a lattice- matched heterostructure consisting of Ge and a ternary $Ge_{1-x-y}Si_xSn_y$ based on Jaros' band offset theory,[12] which is in good agreement with experiment for many heterojunction systems. For example, this theory predicts an average valence band offset, $\Delta E_{v,av} = 0.48$ eV for a Ge/Si heterostructure (higher energy on the Ge side), close to the accepted value of $\Delta E_{v,av} = 0.5$ eV. The basic ingredients of our calculation are the average (between heavy, light, and split-off hole bands) valence band offset between the two materials and the compositional dependence of the band structure of the ternary alloy. For a Ge/α-Sn interface Jaros' theory predicts $\Delta E_{v,av} = 0.69$ eV (higher energy on the Sn side). For the $Ge_{1-x-y}Si_xSn_y$/Ge interface we have used the customary approach for alloy semiconductors, interpolating the average valence band offsets for the elementary heterojunctions Ge/Si and Ge/α-Sn. Thus we used $\Delta E_{v,av}(x,y) = E_{v,av}(GeSiSn) - E_{v,av}(Ge) = -0.48x + 0.69y$ (in eV). Once the average valence band offset is determined, the energies of individual conduction band edges in the $Ge_{1-x-y}Si_xSn_y$ alloy can be calculated relative to those in Ge from the compositional dependence of the spin-orbit splitting of the top valence band states and the compositional dependence of the energy separations between those conduction band edges and the top of the valence band in the alloy.[13] We have assumed that all required alloy energies can be interpolated between the known values for Si, Ge, and α-Sn as

$$E_{GeSiSn}(x,y) = E_{Ge}(1-x-y) + E_{Si}x + E_{Sn}y - b_{GeSi}(1-x-y)x - b_{GeSn}(1-x-y)y - b_{SiSn}xy \quad (1)$$

The bowing parameters b_{GeSi}, b_{GeSn}, and b_{SiSn} have been discussed in Refs. 14 and 15. Finally, for the indirect conduction band minimum near the X-point, Weber and Alonso find $E_X = 0.931 + 0.018x + 0.206x^2$ (in eV) for $Ge_{1-x}Si_x$ alloys. [16] On the other hand, the empirical pseudopotential calculations of Chelikovsky and Cohen place this minimum at 0.90 eV in α-Sn, virtually the same as its value in pure Ge.[17] We thus assume that the position of this minimum in ternary $Ge_{1-x-y}Si_xSn_y$ alloys is independent of the Sn concentration y. The conduction band minima results are shown in Fig.1 for Sn concentrations $0 < y < 0.1$. The Si concentration x was calculated using Vegard's law in such a way that the ternary $Ge_{1-x-y}Si_xSn_y$ is exactly lattice-matched with Ge.

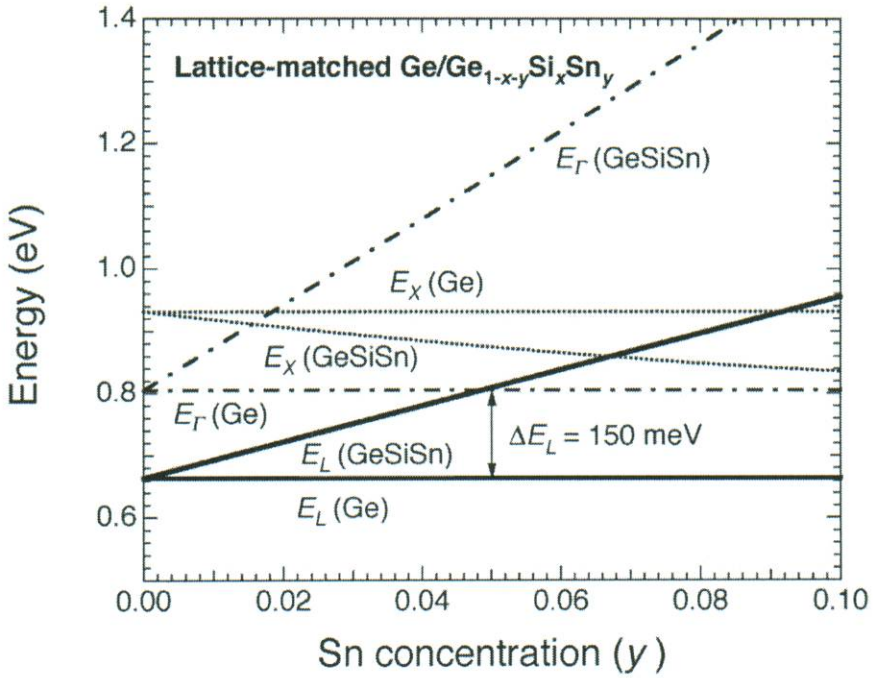

Fig.1 Conduction band minima at L, Γ, X – points of $Ge_{1-x-y}Si_xSn_y$ that is lattice matched to Ge.

It can be seen from Fig.1 that a conduction-band offset of 150 meV at L-valleys can be obtained between lattice-matched Ge and $Ge_{0.76}Si_{0.19}Sn_{0.05}$ alloy while all other conduction-band valleys (Γ, X, etc) are above the L-valley band edge of the $Ge_{0.76}Si_{0.19}Sn_{0.05}$ barrier. This band alignment presents a desirable alloy composition from which a QCL operating at L-valleys can be designed using Ge as QWs and $Ge_{0.76}Si_{0.19}Sn_{0.05}$ as barriers without the complexity arising from other energy valleys.

I.4 $Ge/Ge_{1-x-y}Si_xSn_y$ QCL structure

Using Ge/ $Ge_{0.76}Si_{0.19}Sn_{0.05}$ QWs, we have designed a QCL structure as illustrated in Fig. 2 where only L-valley conduction-band lineups are shown in the potential diagram under an applied electric field of 10 kV/cm. In order to solve the Schrödinger equation to yield subbands and their associated envelope functions, it is necessary to determine the effective mass m_z along

the (001) growth direction (z) within the constant-energy ellipsoids at the L-valleys along the (111) direction which is tilted with respect to (001). Using the L-valley principal transverse effective mass $m_t = 0.08m_o$, and the longitudinal effective mass $m_l = 1.60m_o$, we obtain $m_z = (2/3m_t + 1/3m_l)^{-1} = 0.12m_o$ where m_o is the free electron mass. The squared magnitudes of all envelope functions are plotted at energy positions of their associated subbands. As shown in Fig.2, each period of the QCL has an active region for lasing emission and an injector region for carrier transport. These two regions are separated by a 30 Å barrier. The active region is constructed with 3 coupled Ge QWs that give rise to three subbands marked 1, 2, and 3. The lasing transition at the wavelength of 49 μm is between the upper laser state 3 and the lower laser state 2. The injector region consists of 4 Ge QWs of decreasing well widths all separated by 20Å $Ge_{0.76}Si_{0.19}Sn_{0.05}$ barriers. The depopulation of lower state 2 is through scattering to state 1 and to the miniband downstream formed in the injector region. These scattering processes are rather fast because of the strong overlap between the involved states. Another miniband in the injector region formed of quasi-bound states is situated 45 meV above the upper laser state 3, effectively preventing escape of electrons from upper laser state 3 into the injector region.

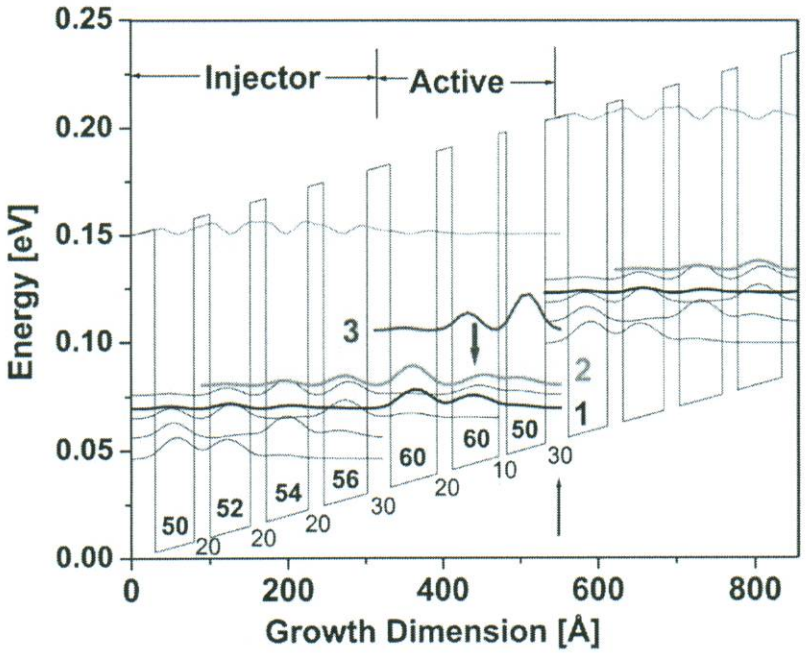

Fig.2 L-valley conduction band profile and squared envelope functions under an electric field of 10kV/cm. Layer thicknesses in angstrom are marked with bold numbers for Ge QWs and regular for GeSiSn barriers. Array marks the injection barrier.

I.5 QCL analysis

The nonradiative transition rates between different subbands in such a low-doped nonpolar material system with low injection current should be dominated by deformation-potential scattering of nonpolar optical and acoustic phonons. For this Ge-rich structure, we have

used bulk-Ge phonons for calculation of the scattering rate to yield lifetimes for the upper laser state τ_3 and the lower laser state τ_2, as well as the 3→2 scattering time τ_{32}.[18] They are shown in Fig.3 as a function of operating temperature. These lifetimes are at least one-order of magnitude longer than those of III-V QCLs owing to the nonpolar nature of GeSiSn alloys.

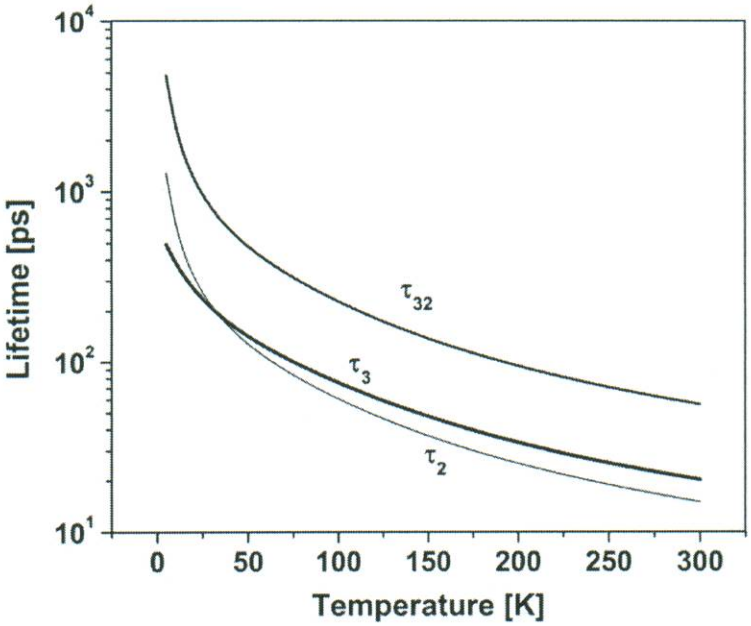

Fig.3 Lifetimes for the upper laser state τ_3 and the lower laser state τ_2, and the 3→2 scattering time τ_{32} as a function of operating temperature.

The necessary condition for population inversion $\tau_{32} > \tau_2$ is satisfied throughout the temperature range. Using these predetermined lifetimes in the population rate equation under current injection:

$$\begin{cases} \dfrac{\partial N_3}{\partial t} = \dfrac{\eta J}{e} - \dfrac{N_3 - \bar{N}_3}{\tau_3} \\ \dfrac{\partial N_2}{\partial t} = \dfrac{N_3 - \bar{N}_3}{\tau_{32}} - \dfrac{N_2 - \bar{N}_2}{\tau_2} \end{cases} \tag{2}$$

where e is the electron charge, N_i $(i = 2, 3)$ is the area carrier density per period in subband i under injected current density J with an injection efficiency η, and $\bar{N}_i$ is the area carrier density per period due to thermal excitation of n-doping. Solving the above rate equation at steady state yields population inversion

$$N_3 - N_2 = \tau_3 (1 - \frac{\tau_2}{\tau_{32}}) \frac{\eta J}{e} - (\bar{N}_2 - \bar{N}_3) . \tag{3}$$

which can be then used to evaluate the optical gain of the TM polarized mode as[19]

$$g = \frac{2e^2\hbar |<3|p_z|2>|^2}{\varepsilon_o c n m_z^2 \gamma L_p (\hbar\omega_L)} [\tau_3 (1 - \frac{\tau_2}{\tau_{32}}) \frac{\eta J}{e} - (\bar{N}_2 - \bar{N}_3)] \quad (4)$$

where ε_o is the permittivity in vacuum, c the speed of light in vacuum, $\hbar$ the Planck constant, and $<3|p_z|2>$ the momentum matrix between the two laser states. Other parameters are as follows: index of refraction n =3.97, lasing transition energy $\hbar\omega_L$ = 25 meV, full width at half maximum γ = 10 meV, length of one period of the QCL L_p = 532 Å, area doping density per period of 10^{10} / cm^2, and unit injection efficiency $\eta = 1$.

The operations of QCL require proper waveguide structures that effectively confine the stimulated emission in the active regions where lasing takes place. For lasing wavelengths in excess of 10μm there is no easy way to accomplish this goal. The difference in the indices of refraction of different semiconductors in the far-IR range is typically small. It is therefore necessary to explore other media with large contrast of indices of refraction. Metals with negative indices of refraction offer such a property. As a result, plasmon waveguides using metal as the cladding layers for long wavelength QCLs have been routinely used to provide sub-wavelength confinement. Here we have considered the plasmon waveguide using Au as cladding layers to provide the confinement for the active region of the Ge/ $Ge_{0.76}Si_{0.19}Sn_{0.05}$ QCL as illustrated in Fig.4. Such a plasmon waveguide supports only TM modes with a mode profile shown in Fig.5.

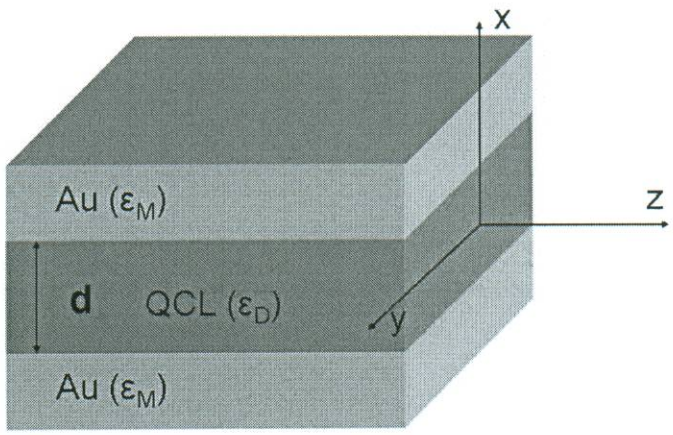

Fig.4 Illustration of the plasmon waveguide using Au as cladding layers to confine the active region of the Ge/ $Ge_{0.76}Si_{0.19}Sn_{0.05}$ QCL.

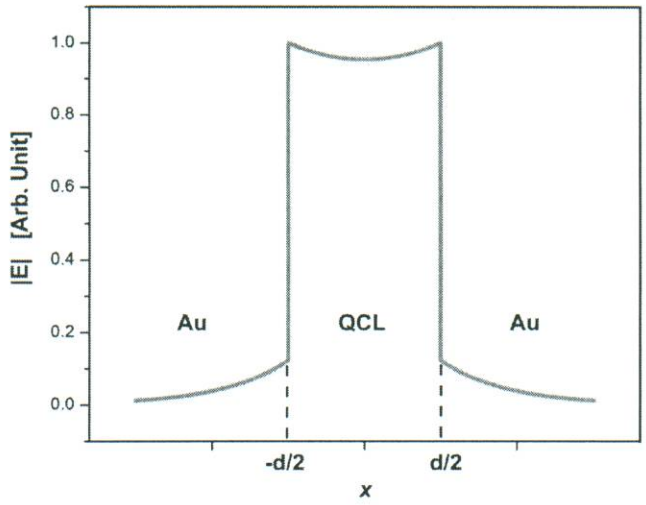

Fig.5 Profile of a TM mode supported by the plasmon waveguide with Au as cladding layers for the Ge/ $Ge_{0.76}Si_{0.19}Sn_{0.05}$ QCL.

We have simulated the TM-polarized mode in a QCL structure of 40 periods that is confined by double-Au-plasmon waveguide and obtained near unity optical confinement $\Gamma \approx 1.0$ and waveguide loss $\alpha_w = 110/\text{cm}$. Assuming a mirror loss $\alpha_m = 10/\text{cm}$ for a typical cavity length of 1mm, the threshold current density J_{th} can be calculated from the balancing relationship, $\Gamma g_{th} = \alpha_w + \alpha_m$. The result is shown in Fig.6 for J_{th} that ranges from 22A/cm^2 at 5K to 550A/cm^2 at 300K. These threshold values are lower than those of III-V QCLs as a result of the longer scattering times due to nonpolar optical phonons.

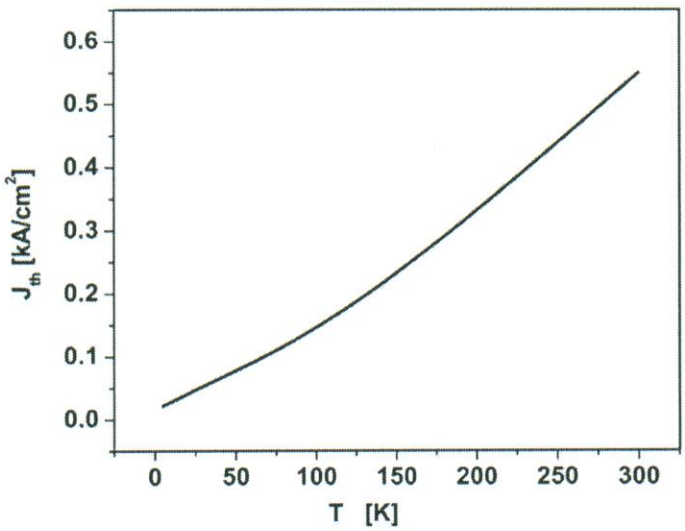

Fig.6 Ge/ $Ge_{0.76}Si_{0.19}Sn_{0.05}$ QCL threshold current density as a function of operating temperature.

I.6 Conclusions

We have designed a $Ge/Ge_{0.76}Si_{0.19}Sn_{0.05}$ QCL that operates at *L*-valleys of the conduction band. According to our estimation of the band lineup, this particular alloy composition gives a "clean" conduction band offset of 150meV at *L*-valleys with all other energy valleys conveniently out of the way. All QCL layers are lattice matched to a Ge buffer layer on a Si substrate and the entire structure is therefore strain free. The electron effective mass along the growth direction is much lighter than that of heavy holes bringing a significant improvement in tunneling rates and oscillator strengths. The lasing wavelength of this device is 49 μm. With different GeSiSn alloy compositions that are lattice matched to Ge, QCLs can be tuned to lase at other desired wavelengths. Lifetimes determined from the deformation potential scattering of nonpolar optical and acoustic phonons are at least an order of magnitude longer than those in III-V QCLs with polar optical phonons, leading to a reduction in threshold current density and the possibility of room temperature operation.

II. Phonon Waveguides

In recent years significant progress has been achieved in development of efficient sources and detectors of far-IR radiation in the range of 12-30 μm. These devices, especially quantum cascade lasers (QCLs) require efficient waveguiding structures capable of providing high degree of optical confinement with low loss. Unfortunately at wavelengths in excess of 10μm there is no easy way to accomplish this goal. The difference in the indices of refraction of different semiconductors in the far-IR range is typically small, unless one ventures close to one of the lattice resonances where index is large. Unfortunately, in the vicinity of the resonance lattice absorption losses inevitably increase and the laser threshold becomes very high. At any rate, even with a reasonably large index contrast a typical dielectric waveguide for long wavelength radiation would have to be very thick, making the growth and fabrication difficult and expensive. In this project, we have studied a special waveguide that uses the property of interface phonon polaritons to confine far-infrared radiation within a sub-wavelength semiconductor layer. We identify spectral operating regions within the Restrahlen band of a cladding layer that offers advantages over both traditional dielectric and metal clad waveguides. We show that proposed waveguides can be used for far-infrared low-threshold quantum cascade lasers.

II.1 Plasmon vs. phonon waveguides

As we have discussed earlier, plasmon waveguides are typically used in place of dielectric waveguides. In such a metal clad waveguide capable of supporting surface plasmon polariton (SPP) modes where the fields are evanescent in both dielectric core and metal cladding,[20,21] the thickness of active waveguide core thus can be made much smaller than the wavelength. Regrettably, a metal clad waveguide is not entirely problem free. First of all, metal is strongly absorptive in the far IR region. Second, it is far from trivial to deposit metal layers on both sides of the waveguide. For this reason one often has to resort to use of highly doped semiconductors in place of metal,[22,23] but in this arrangement high free carrier absorption becomes a significant factor.

The origin of strong absorption losses in metal and highly doped semiconductor can be traced to extremely fast energy relaxation rates of electrons – it is ~ 10fs in Au and ~ a few 100fs in the highest quality GaAs. One would like to identify some transitions that are less prone to scattering. Such transition can be associated with optical phonons that are known to have scattering times on the order of a few picoseconds. This is especially true for the binary semiconductors with large discrepancy between masses and electron affinities of the ions, such as SiC and GaN. In GaN optical phonons have a long lifetime ~3ps [24] primarily because its energy is more than two times higher than the energy of two acoustic phonons. As a result, the usual dominant decay channel in which one optical phonon splits into two acoustic phonons[25] is forbidden in GaN. Furthermore, GaN bond is highly ionic and thus its vibrations have very large oscillator strength. Due to strong optical phonon resonance there exists a Restrahlen region in the far-IR where the dielectric constant is actually negative and the material behaves just like a metal. Therefore, at the interface between two semiconductors, one of which is in Restrahlen region and the other not, there exists a surface polariton TM mode which exponentially decays into both materials. This mode can be used to provide desired confinement with low loss. In this part of the project we developed the idea that uses surface phonon polariton modes to provide the waveguide in quantum cascade lasers (QCLs) and other far-IR devices made of III-V or II-VI compound semiconductors.

II.2 Design of phonon waveguides

We considered a structure consisting of GaAs-based active layer and GaN cladding. Since GaAs-based QCLs cannot operate in the frequency region that is either inside or just above its own Restrahlen band, and the Restrahlen band of GaN is far above that of GaAs, we compare two GaAs-based QCLs operating in the Restrahlen region of GaN. One uses GaN as cladding, the other uses Au as shown in Fig.7. Both waveguides will support TM modes with an electric field

$$\mathbf{E} = \begin{cases} \dfrac{\cosh(kd/2)}{\varepsilon} E_o (j\beta\hat{\mathbf{x}} + q\hat{\mathbf{z}}) e^{-q(x-d/2)} e^{j(\beta z-\omega t)}, & x > d/2 \\ E_o [j\beta \cosh(kx)\hat{\mathbf{x}} - k \sinh(kx)\hat{\mathbf{z}}] e^{j(\beta z-\omega t)}, & |x| < d/2 \\ \dfrac{\cosh(kd/2)}{\varepsilon} E_o (j\beta\hat{\mathbf{x}} - q\hat{\mathbf{z}}) e^{q(x+d/2)} e^{j(\beta z-\omega t)}, & x < -d/2 \end{cases} \quad (1)$$

where the complex wave vectors $\beta = \beta' + j\beta''$ and k are related by the dispersion relation $k^2\left[\varepsilon^2 \tanh^2(kd/2) - 1\right] = 1 - \varepsilon$ with $\varepsilon = \varepsilon_{P,M} / \varepsilon_D$ according to the boundary conditions, and d is the waveguide active core width. The dielectric function of GaN in the Restrahlen band can be approximated as $\varepsilon_p = \varepsilon_\infty \left(1 + \dfrac{\omega_{LO}^2 - \omega_{TO}^2}{\omega_{TO}^2 - \omega^2 - j\omega\gamma_p}\right)$, and that of Au as $\varepsilon_M = 1 - \dfrac{\omega_p^2}{\omega^2 + j\omega\gamma_M}$ according to Drude model. The Restrahlen band of GaN is between $\hbar\omega_{TO} = 67.6\,\text{meV}$, and $\hbar\omega_{LO} = 89.7\,\text{meV}$ with $\gamma_p = 0.1\,\text{meV}$.[26] For Au, the plasmon frequency corresponds to $\hbar\omega_M = 8.11\,\text{eV}$ with $\gamma_M = 65.8\,\text{meV}$.[27]

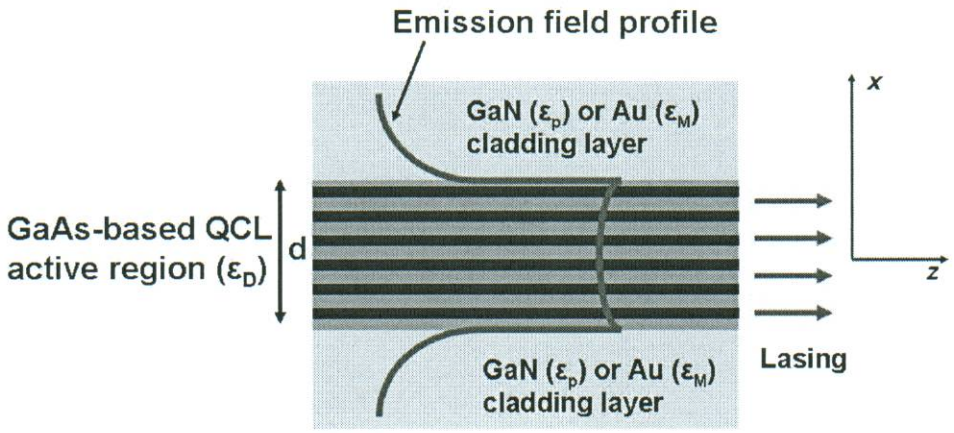

Fig. 7 Illustration of a GaAs-based active region waveguide with either GaN or Au as cladding operating in the Restrahlen band of GaN.

We compared the threshold optical gain required to achieve lasing in QCL based on two waveguides with an active region thickness of 1μm, using $g_{th} = (\alpha_w + \alpha_m)/\Gamma$, where the optical confinement factor $\Gamma = \int_{-d/2}^{d/2} |E|^2 dx / \int_{-\infty}^{\infty} |E|^2 dx$ is the ratio of the emission field intensity profile within the waveguide active core to that of overall waveguide, α_m is the mirror loss, and α_w is the waveguide loss which can be obtained by $\alpha_w = 2\beta''$. By keeping the thickness of active waveguide core at $d = 1.0\mu m$ which is much less than the operating wavelength, we calculate the optical confinement factor (Fig. 8) and the waveguide loss (Fig. 9) of the two waveguides. If can be seen from Figs. 8 and 9 that while the Au surface Plasmon polariton waveguide provides better optical confinement, the GaN surface phonon polariton waveguide has an advantage of a lower loss.

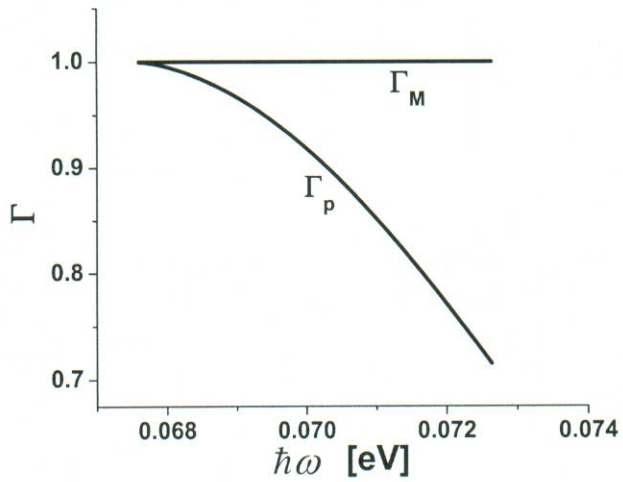

Fig. 8 Comparison of optical confinement factors between the GaAs/GaN and GaAs/Au waveguides ($d = 1\mu m$) within the Restrahlen band of GaN.

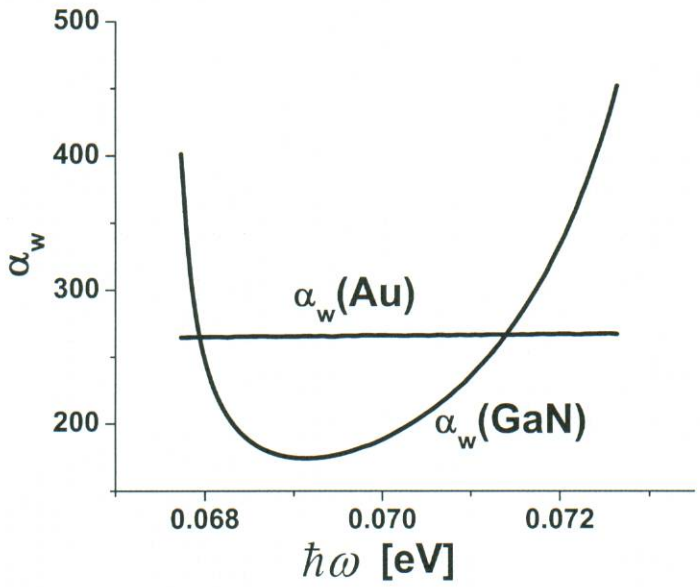

Fig. 9 Comparison of waveguide loss of the GaAs/GaN and GaAs/Au waveguides ($d = 1\mu m$) within the Restrahlen band of GaN.

For a fair comparison, we have calculated the ratio of threshold gain between the two waveguides

$$\frac{g_{th,P}}{g_{th,M}} = \frac{\Gamma_M}{\Gamma_P}\frac{2\beta_P'' + \alpha_m}{2\beta_M'' + \alpha_m}. \tag{2}$$

The result is plotted in Fig.10 as a function of the operating wavelength within the Restrahlen band of GaN for a range of values of mirror loss α_m. It can be seen from Fig.10 that within a narrow photon energy range from 68.0 to 70.7meV (λ = 17-18μm), the threshold in GaN-clad QCL is reduced relative to the Au-clad waveguide. While the window itself is a narrow one, the nearly two-fold reduction of the threshold is substantial.

II.3 Conclusions

In summary, we have studied the characteristics of waveguide using highly-reflective semiconductor in the Restrahlen band as cladding layers. With its negative dielectric constant in the Restrahlen band, the cladding semiconductor supports surface phonon polaritons that behave like surface Plasmon polaritons in a metal-dielectric waveguide, but with less absorption loss. Using the example of GaAs active region confined by either GaN or Au cladding layers, we have compared the optical confinement factor and waveguide loss between the two different structures, and have identified spectral operating region within the Restrahlen band of GaN that offers advantages over both traditional dielectric waveguide and metal waveguides.

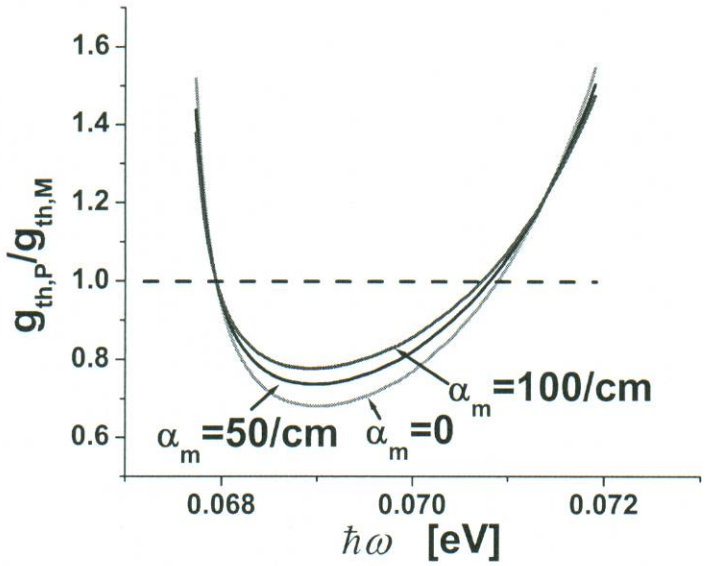

Fig. 10 Ratio of threshold optical gain between GaN Restrahlen and Au plasmon waveguide as a function of photon energy for several values of mirror loss.

References

1. G. Sun, L. Friedman, and R. A. Soref, Appl. Phys. Lett. **66**, 3425 (1995).
2. G. Dehlinger, L. Diehl, U. Gennser, H. Sigg, J. Faist, K. Ensslin, D. Grützmacher, and E. Müller, Science **290**, 2277 (2000).
3. I. Bormann, K. Brunner, S. Hackenbuchner, G. Abstraiter, S. Schmult, and W. Wegscheider, Appl. Phys. Lett. **80**, 2260 (2002).
4. S. A. Lynch, R. Bates, D. J. Paul, D. J. Norris, A. G. Cullis, Z. Ikonić, R. W. Kelsall, P. Harrison, D. D. Arnone, and C. R. Pidgeon, Appl. Phys. Lett. **81**, 1543 (2002).
5. K. Driscoll and R. Paiella, Appl. Phys. Lett. **89**, 191110 (2006).
6. R. A. Soref and C. H. Perry, J. Appl. Phys. **69**, 539 (1991).
7. D. W. Jenkins and J. D. Dow, Phys. Rev. B **36**, 7994 (1987).
8. G. He and H. A. Atwater, Phys. Rev. Lett. **79**, 1937 (1997).
9. J. Menéndez and J. Kouvetakis, Appl. Phys. Lett. **85**, 1175 (2004).
10. M. Bauer, C. Ritter, P. A. Crozier, J. Ren, J. Menéndez, G. Wolf, and J. Kouvetakis, Appl. Phys. Lett. **83**, 2163 (2003).
11. M. A. Wistey, Y.-Y. Fang, J. Tolle, A. V. G. Chizmeshya, and J. Kouvetakis, Appl. Phys. Lett. **90**, 082108 (2007)
12. M. Jaros, Phys. Rev. B **37**, 7112 (1988).
13. C. G. Van de Walle, Phys. Rev. B **39**, 1871 (1989).
14. V. R. D'Costa, C. S. Cook, A. G. Birdwell, C. L. Littler, M. Canonico, S. Zollner, J. Kouvetakis, and J. Menendez, Phys. Rev. B **73**, 125207 (2006).
15. V. R. D'Costa, C. S. Cook, J. Menendez, J. Tolle, J. Kouvetakis, and S. Zollner, Solid State Commun. **138**, 309 (2006).
16. J. Weber and M. I. Alonso, Phys. Rev. B **40**, 5683 (1989).
17. M. L. Cohen and T. K. Bergstresser, Phys. Rev. **141**, 789 (1966).
18. B. K. Ridley, *Electrons and Phonons in semiconductor Multiplayers* (Cambridge University Press, Cambridge, 1997), Chap. 1.
19. S. K. Chun and K. L. Wang, Phys. Rev. B. **46**, 7682 (1992).
20. K. Unterrainer, R. Colombelli, C. Gmachl, F. Cappasso, H. Y. Hwang, A. M. Sergent, D. L. Sivco, and A. Y. Cho, Appl. Phys. Lett. **80**, 3060 (2002)
21. B. S. Williams, S. Kumar, H. Callebaut, Q. Hu, and J. L. Reno, Appl. Phys. Lett. **83**, 2124 (2003)
22. M. Rochat, M. Beck, J. Faist, U. Oesterle, Appl. Phys. Lett. **78**, 1967 (2001)
23. R. Köhler, A. Trediccuci, F. Beltram, H. E. Beere, E. H. Linfield, A. G. Davies, D. A. Ritchie, R. C. Lotti, and F. Rossi, Nature **417**, 156 (2002)
24. A. Matulionis, J. Liberis, I. Matulioniene˙, M. Ramonas, L. F. Eastman, J. R. Shealy, V. Tilak, and A. Vertiatchikh, Phys. Rev. B **68**, 035338 (2003)
25. P. G. Klemens, Phys. Rev. **148**, 845 (1966)
26. Semiconductors: group-IV and III-V compounds, Editor: O. Madelung, (Springer-Verlag, Berlin, Heidelberg, 1991) p.86

List of Symbols, Abbreviations, and Acronyms

THz	Terahertz
QCL	Quantum cascade laser
QW	Quantum well
IST	Intersubband transitions
SPP	Surface plasmon polariton
IR	Infrared